Analysis of Traffic Flow at Complex Congested Arterials

PANOS G. MICHALOPOULOS

A dynamic macroscopic methodology for analyzing traffic flow at congested intersections and arterial streets is presented in this paper. This includes complexities frequently encountered in practice such as turning and optional lanes, sinks and sources, and spillback effects. The dynamics of interrupted flow under both sign and signal control are treated in an integrated fashion by considering the coupling effects of the main and side street flows. Compressibility is inherently included in the state equations employed; therefore, dispersion and compression characteristics are built into the analysis. The proposed methodology is particularly applicable to severely congested networks where spillbacks must be taken into account. Implementation of the state equations is performed numerically; this allows inclusion of stochastic and heuristic aspects for treating phenomena difficult to deal with macroscopically. The modelling and numerical treatment employed is easily implementable to microcomputers.

Modelling of interrupted traffic flow at signalized intersections and arterial streets is frequently needed in traffic engineering practice for simulation and control or simply for analyzing a situation during the planning and design stages. More often than not this is accomplished in a macroscopic fashion to minimize the computations and obtain a better understanding of the overall behavior of the process being analyzed; this is particularly the case as the size of the network increases. However, despite the attractiveness of macroscopic models, rigorous and comprehensive dynamic treatment of complexities most frequently encountered in practice is still lacking. Such complexities include turning or optional lanes, spillback effects, unsignalized side streets merging to or diverging from the main stream flow, macroscopic treatment of actuated signals, and friction effects. The problem is more acute at high volume streets where two-dimensional modelling is needed for describing the formation and dissipation of queues and spillbacks in time and space and for taking into account the effects of downstream disturbances on upstream flow.

In view of the need for improved dynamic macroscopic modelling of congested interrupted flow, a new approach is presented in this paper. The modelling employed is two dimensional (time and space), takes compressibility into account (dispersion and compression), and is particularly recommended for medium to heavy flow situations. Moreover, it considers the interactions of side streets and turning lanes and the effects of compression and spillbacks caused by downstream congestion. Finally, it applies to sign and signal control and to isolated intersections and arterials. The proposed methodology is numerical, i.e., it proceeds by discretizing the time-space domain in small increments and should be more intensive computationally than existing one-dimensional models used in practice. However, it is perfectly suitable for microcomputer implementation because it requires substantially less memory and computational effort than microscopic modelling.

The proposed methodology could be called "mesoscopic" as it allows inclusion of statistical and heuristic aspects for treating certain phenomena in a manner similar to a microscopic approach.

In what follows, a brief theoretical background on the state equations employed is presented with a general numerical solution method for their implementation. This is followed by the treatment of simple isolated signalized intersections. Due to space limitations, only a summary of details such as treatment of sinks and sources, exclusive turning lanes, and traffic actuated control is presented here. Extension to coordinated intersections and implementation to exemplary situations are included to demonstrate the applicability of the proposed modelling.

BACKGROUND

Macroscopic analysis of traffic stream flow requires estimation of the three basic variables, i.e., density (k), speed (u), and flow rate (q), on every point of the roadway at all times during the analysis period. From these variables the measures of effectiveness (delays, stops, total travel, and total travel time) can be derived. The most rigorous approach for calculating q, k, and u in both time and space is by employing the law of conservation with an equilibrium speed-density or flow-density relationship to take compressibility (compression and dispersion) into account (*1*). An even more sophisticated treatment is to also consider acceleration and inertia of a traffic mass (*2*, *3*), but although this approach is plausible, it has not shown significant advantages at congested flows, adding only complexity to the analysis. The methodology described here, however, can easily be generalized to include these effects (*5*).

Analytical implementation of the law of conservation to isolated and coordinated intersections by taking time, space, and compressibility into account has been developed recently (*5–7*). The advantage of these analytical results is that they visually depict the effects of downstream disturbances on upstream flow. Thus, they provide a good insight on the formation and dissipation of queues and congestion in time and space; they also demonstrate (*7*) that platoon dispersion and

Department of Civil and Mineral Engineering, University of Minnesota, Minneapolis, Minn. 55455.

compression is inherent in this modelling, i.e., it does not have to be induced externally. The dynamics of platoons and their behavior can in addition be studied analytically (*7*) for better understanding of arterial flow behavior. A disadvantage of the analytical solution lies in the oversimplifications needed in the derivation. These include simple initial flow conditions, arrival and departure patterns, absence of sinks or sources, and uncomplicated flow-concentration relationships. Most important, complexities frequently encountered in real situations such as turning lanes and side streets cannot be treated analytically. As in similar problems of compressible flow, these difficulties can be resolved by developing numerical solutions for the state equations.

The methodology proposed here is computational rather than analytical. This eliminates the disadvantages mentioned above by allowing inclusion of complexities one is likely to encounter in practice (turning lanes, sinks and sources, and spillbacks) and employment of realistic arrival and departure patterns, *u-k* models as well as empirical considerations. Numerical computation of k, u, and q proceeds by discretizing the roadway under consideration into small increments Δx (in the order of 30 to 150 ft) and updating the values of these traffic flow variables on each node of the discretized network at consecutive time increments Δt (in the order of 1 sec or so).

Space discretization of a simple signalized traffic link without side streets is presented in Figure 1 in which the dashed segments represent dummy links necessary in the modelling of subsequent sections. It should be stressed that this discretization is only made for computational purposes, i.e., it is not physical. Referring to the solid segments, density on any node j except the boundary ones (i.e., 1 and j) at the next time step $n + 1$ is computed from density in the immediately adjacent links (both upstream and downstream $j - 1$ and $j + 1$, respectively) at the current time step n according to the relationship

$$k_j^{n+1} = \frac{1}{3}(k_j^n + k_{j+1}^n + k_{j-1}^n) - \frac{\Delta t}{2\Delta x}(q_{j+1}^n - q_{j-1}^n) \qquad (1)$$

in which

k^n_j, q^n_j = density and flow rate, respectively, on node j at $t = t_0 + n\Delta t$;
t_0 = initial time; and
Δt, Δx = time and space increments, respectively, such that $\Delta x/\Delta t >$ free flow speed.

Once density is determined, speed at $t + \Delta t$ (i.e., at $n + 1$) is obtained from the equilibrium speed density relationship $u_e(k)$, i.e.,

$$u_j^{n+1} = u_e(k_j^{n+1}) \qquad (2)$$

For instance, if Greenshields' (*8*) linear model is adopted, then

$$u_j^{n+1} = u_f\left(1 - \frac{k_j^{n+1}}{k_{\text{jam}}}\right) \qquad (2a)$$

where u_f is the free flow speed and k_{jam} the jam density. It should be stressed that Equation 2 is applicable for any speed density model including discontinuous ones; if an analytical expression is not available, then u can easily be obtained numerically from the $u - k$ curve. Finally, flow at $t + \Delta t$ is obtained from the fundamental relationship

$$q_j^{n+1} = k_j^{n+1} u_j^{n+1} \qquad (3)$$

in which the values of k and u are first obtained from Equations 1 and 2. As later sections suggest, the measures of effectiveness can be derived from k, u, and q.

The above solution requires definition of the initial state of the system, i.e., the values of k, u, and q at $t = t_0$ as well as boundary conditions, i.e., k and q at $j = 1$ and $j = J$ (upstream end of the link and stopline, respectively). However, this is essential for analyzing flow regardless of the modelling and solution method, i.e., arrivals and departures at the boundaries and initial flows must always be specified. For practical implementation of Equations 1, 2, and 3 one only needs to specify arrival and departure flow rates; density at $j = 1$ and $j = J$ is obtained from the equilibrium q-k model. It should be noted that Equation 1 does not take into account generation or dissipation of cars; this detail is discussed later. Finally, the discretization of Figure 1 and numerical solution of this section assume all space increments Δx are equal. The case of variable space discretization is presented later; however, regardless of the discretization scheme the relationship $\Delta x/\Delta t \rangle u_f$ must be maintained at all times for convergence.

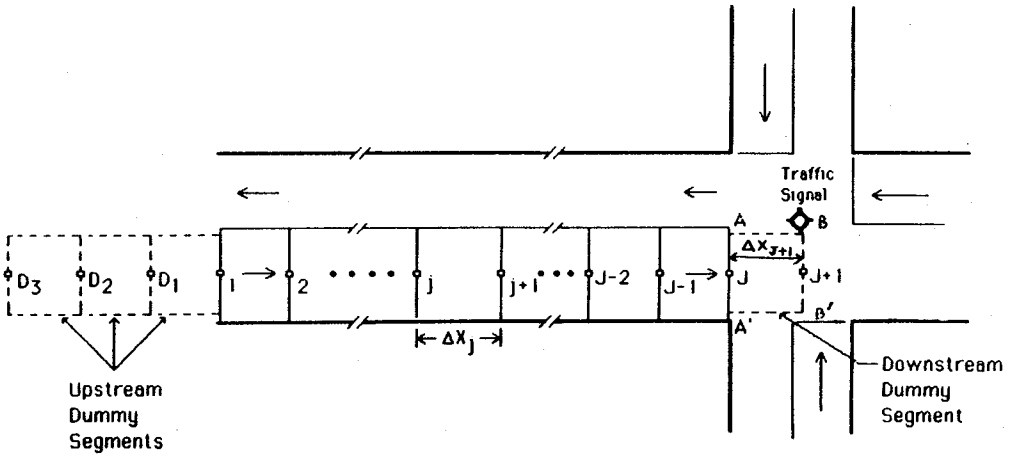

FIGURE 1 Space discretization of a simple link.

ISOLATED INTERSECTIONS

The basic methodology of the previous section (Equations 1–3) is directly applicable to simple isolated signalized intersections without turning lanes or sinks and sources (Figure 1). Proper definition of the initial and boundary conditions is crucial for accuracy and emulating the particular situation at hand. Initial conditions depend on the state of the signal indication on the approach under consideration, and unless an actual measurement is available, a simplified assumption can be made. For instance, one could initially assume that the approach is empty at $t = 0$ (i.e., $k_j^0 = 0$ at all nodes) and following an initialization interval use the flow conditions at the end of this interval as initial conditions. Another simple alternative is to assume that at $t = 0$ the signal turns green on the approach under consideration on which an initial queue exists; if flow within the queue is uniform, then on the nodes within the queue $q_j^0 = 0$ and $k_j^0 = k_{\text{jam}}$ while behind the queue uniform arrival flow conditions, i.e., $q_j^0 = q_1^0$ and $k_j^0 = k_1^0$, can be hypothesized. In the testing presented in later sections initial conditions are variable.

Upstream and downstream boundary conditions in case of real time applications of the proposed methodology can be obtained on-line from loop detectors, i.e., by measuring actual arrivals and departure flow rates on nodes 1 and J, respectively. In simulation, these rates can be obtained from the probability distribution one is willing to accept. In some applications, however, it is desirable to reduce the computations related to the generation of stochastic boundary conditions. This is most easily accomplished at the downstream boundary where the variability of departures is less pronounced for the majority of the cycle due to the presence of the traffic signal. For instance, the simplest modelling alternative is the one frequently used in practice, according to which flow at $j = J$ during the effective green time equals saturation flow as long as there is a queue (i.e., $q_j^{n+1} = q_{\max}$ = saturation flow) and to arrival flow when the queue dissipates (i.e., $q_j^{n+1} = q_{J-1}^n$). During the effective red interval flow equals zero (right turns on red can also be considered as will be seen later). Only one state variable (flow, density, or speed) need be specified at each boundary; the remaining are obtained from the q-k or u-k model and the fundamental relationship $q = ku$.

The above and other simple common options for defining boundary conditions were tested extensively using a data base generated by the most recent version of NETSIM (*9*) (1986 version). Based on this experimentation, effective simplified modelling of the boundary conditions was developed and is described next.

With respect to downstream boundary conditions (stop line), during the green interval, one dummy segment of variable length is introduced immediately downstream of the stop line. This segment is shown with dashed lines in Figure 1. The introduction of this dummy segment smooths out the discharge pattern at the stop line during green, so the actual boundary during green is not the stop line but the line $B'B$ (dummy node $J + 1$) in Figure 1. At the start of green, free flow conditions are assumed at the dummy node, i.e., $k_{J+1}^0 = 0$ and $u_{J+1}^0 = u_f$ while at the stop line $k_J^0 = k_{\text{jam}}$ and $u_J^0 = 0$. The length of the dummy segment ΔX_{J+1} at the start of green equals Δx, where Δx is the common discretization length used for the entire link. At every time step during green, the downstream boundary $J + 1$ is determined from the dynamics of flow propagation, i.e., the dummy link length is computed from the speed at which the traffic is moving at the stop line during the previous time step; thus,

$$\Delta x_{J+1}^{n+1} = u_J^n * \Delta t \tag{4}$$

The flow at the pseudo boundary $J + 1$ (dummy node) equals the arrival flow, i.e., $q_{J+1}^{n+1} = q_J^n$ and $k_{J+1}^{n+1} = k_J^n$, while in all the remaining nodes, including the stop line, flow is determined from Equations 1–3. Here the variable dummy link requires generalization of Equation 1 for calculating flow at the stop line. This equation, including generation terms (not needed for the stop line), becomes

$$k_j^{n+1} = \frac{k_{j+1}^n \Delta x_j + k_{j-1}^n \Delta x_{j+1}}{\Delta x_j + \Delta x_{j+1}} - \frac{\Delta t(q_{j+1}^n - q_{j-1}^n)}{\Delta x_j + \Delta x_{j+1}} + \frac{\Delta t(g_{j+1}^n \Delta x_j + g_{j-1}^n \Delta x_{j+1})}{\Delta x_j + \Delta x_{j+1}} \tag{5}$$

where g_j^n represents the generation rate in segment j at the nth time step. When there is no generation from side streets, then g_j^n is zero and the last term of Equation 5 vanishes.

The above modelling implies no congestion downstream of the intersection; this event can be taken into account as in congested coordinated intersections described later. During amber time, the dummy segment is not needed, i.e., the stop line becomes the downstream boundary. Flow at this boundary reduces rapidly with time; it was found experimentally that linear reduction of flow at the stop line during amber is sufficient. Thus during yellow, flow at $j = J$ is

$$q_J(t) = q_J(t_g) * \left[1 - \frac{t - t_g}{t_y - t_g}\right] \qquad t_g < t \leq t_y \tag{6}$$

where

t_g = end of green,
t_y = end of yellow, and
$q_J(t)$ = flow at the stop line at t.

From Equation 6, density during yellow is computed from

$$k_J(t) = k_e\,[q_J(t)] \qquad t_g < t \leq t_y \tag{7}$$

where $k_e(q)$ is the equilibrium k-k relationship. This relationship, however, yields in general two values for k corresponding to a single q value; care should be exercised to select the one corresponding to the congested flow because at the start of yellow congestion begins to emanate from the stop line. Finally, during red, zero flow conditions prevail at the stop line, i.e., $k_J^{n+1} = k_{\text{jam}}$ and $q_J^{n+1} = 0$. If right turns on red are allowed, then $q_J^{n+1} \neq 0$, and this rate can either be specified or determined as in the side street flow case described in the following sections.

As mentioned earlier, at isolated approaches (or external network links) flows at the upstream boundary are more difficult to define due to the absence of signals. If no actual measurements are available (possibly on-line) for defining the upstream arrival flow pattern (q_1^{n+1}) in some detail, then at every time step flow must be determined from a statistical distribution when high accuracy is required. The literature on selecting the appropriate distribution is quite extensive and one can select the most appropriate based on personal experience. In the testing performed here the guidelines of Gerlough et al. (*10*) were followed, with very satisfactory results, at least when compared with NETSIM (*9*). Once q_1^{n+1} is spec-

ified, k_1^{n+1} and u_1^{n+1} are determined from the equilibrium relationships employed, i.e., for Greenshields' model (*8*),

$$k_j^{n+1} = 0.5\,[k_{\text{jam}} - (k_{\text{jam}}^2 - 4\,k_{\text{jam}}\,q_1^{n+1}/u_f)^{1/2}] \quad (8)$$

$$u_1^{n+1} = u_f\,(1 - k_1^{n+1}/k_{\text{jam}}) \quad (9)$$

The above definition of the upstream boundary conditions assumes that downstream congestion at the previous time step n does not reach the upstream boundary, i.e., it assumes uncongested upstream flow conditions. When congestion reaches the upstream boundary, the link should be extended artificially by adding dummy segments D_1, D_2, D_3, . . . , D_i as shown with dashed lines in Figure 1. Extension of the upstream boundary at the next time step $n + 1$ can be determined by checking density on the node immediately downstream (i.e., node 2 initially) at n; if this density falls in the congested region of the u-k or q-k curve, then one dummy segment should be added upstream at $n + 1$. The threshold value for determining congestion is k_m = density at capacity; if $k^n{}_{Di-1} \geq k_m$, a new dummy link is added. Boundary conditions at the first upstream dummy node are determined as before, i.e., from Equations 8 and 9. In some instances an upper limit may exist beyond which no dummy segments can be added; this could be the case when an upstream intersection is reached. In such cases the approach in question can no longer be considered isolated, i.e., the two intersections are coupled and should be treated as a system following the guidelines of later sections.

GENERALIZATIONS AND EXTENSIONS

The basic modelling and analysis methodology presented to this point needs further generalizations and extensions for practical implementation to real situations. These include treatment of sinks and sources, turning lanes, spillback effects, multiple lanes, shared lanes, and coordinated intersections. Due to space limitations the methodology for treating these problems is only briefly presented in this section. A detailed presentation can be found elsewhere (*11*).

Sources and Sinks

When sources and sinks exist, the coupling effects of the main and side streets must be considered. This is accomplished by taking the state equations (conservation) of all system components and solving them simultaneously.

In Figure 2, segment S represents the case of a side street source. The state equations of the two components (main and side street) have the general form of Equation 5, but they differ in the generation term; this term is zero on the entire side street and all segments of the main street except the merging segment (node M) where $g \neq 0$. Since the main street has priority, it must be realized that the stop line of the side street is really an internal boundary. The boundary flow condition on node J_s is restricted by the conflicting flow q_M^n at the merging node M; to be sure, q_M^n determines the merging capacity at J_s. This capacity under uncongested main flow conditions was derived experimentally in the form of a curve showing the merging capacity for different main flow conditions. Similar curves can also be found in Tanner's article (*12*), obtained from the *Highway Capacity Manual* (*13*), or derived experimentally. For congested conditions, the maximum merging flow remains constant until nearly jam density, where it decreases gradually to zero. The boundary conditions at node J_s depend on the state of the queue on the side street. Generally, flow at J_s equals merging capacity, if a queue exists

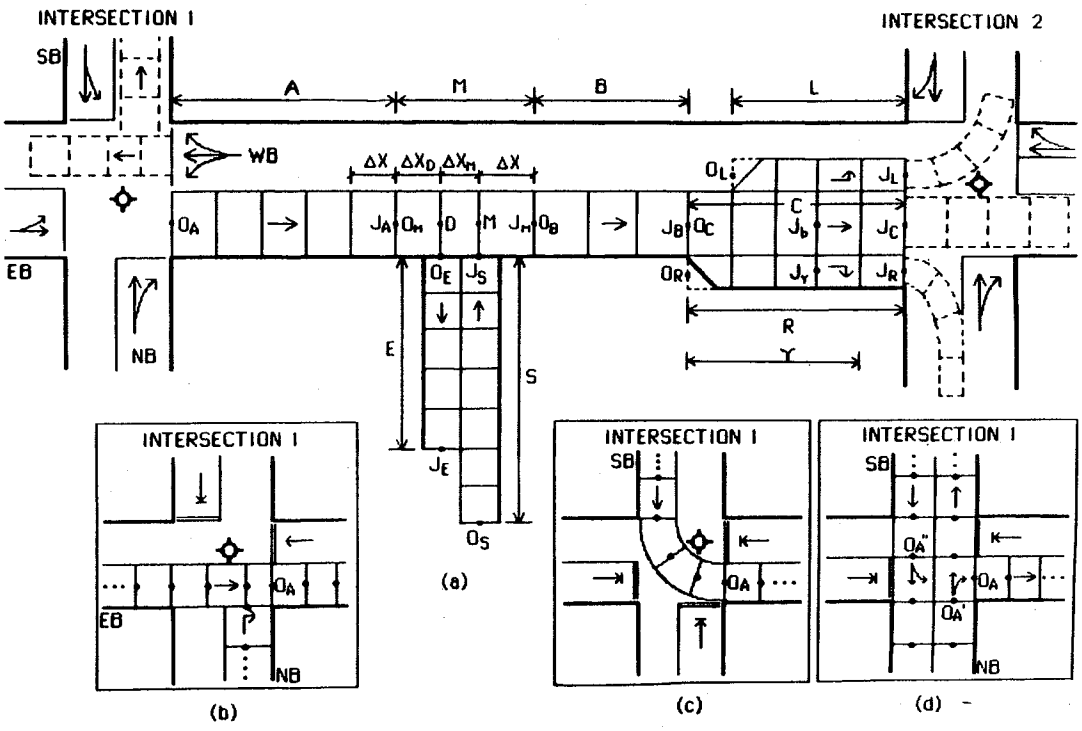

FIGURE 2 Space discretization of a complex arterial link.

on the side street, and equals arrival flow otherwise. Knowing the boundary conditions, Equations 1–3 are applied to determine flow conditions at all nodes of the side street while the generation rate needed for using Equation 5 on the main street is computed from q_{Js}.

In sinks, as in sources, the problem involves determining the flow at the internal boundary O_E (Figure 2). Furthermore, when the side street becomes congested a spillback may occur on the main street; this requires additional modelling. The former problem is resolved by adopting the usual assumption that flow at O_E, q_{OE}^{n+1}, is a known fraction $p = p(t)$ of the main flow at D; however, q_{OE}^{n+1} is restricted by the capacity flow rate $q_{\max}$ at node O_E. Generally, the capacity flow at O_E is lower than the capacity of the remaining nodes of the side street due to possible pedestrian movements and the slower speed of vehicles while turning right. This capacity can be derived from the turning speed, which is the speed at capacity at node O_E. The maximum flow at O_E at every time step is restricted by the maximum speed that can be achieved at O_E by the turning flow. The speed at node $O_E + 1$ influences this speed; therefore, it can be assumed that the free flow speed at O_E is time varying and equals to the speed at $O_E + 1$. The corresponding capacity flow at O_E can be estimated by continuously adjusting the u-k relationship according to this free flow speed. However, due to the earlier maximum turning speed restriction (about 13 ft per sec), $q_{\max}^{n+1}$ cannot exceed this capacity value. Thus, whenever the capacity resulting from the speed at $O_E + 1$ exceeds this value, the latter is imposed. Following determination of $q_{\max}^{n+1}$ at O_E, not only the u-k but also the q-k relationship at this node is adjusted accordingly. When congestion is encountered on the side street, the diverging node D becomes an internal boundary in addition to the boundary O_E. Therefore, the flow at D, q_D^{n+1}, is restricted by the through-portion flow $(1 - p)q_D^n$, which is allowed to proceed on node D. If congestion exists on the side street, the flow at D will decrease, and density will be increasing accordingly because the dissipation rate will decrease. As a result, congestion will begin to build up behind node D and a spillback will occur.

The simultaneous presence of a source and a sink (Figure 2) necessitates consideration of all three flows, namely the through, merging (from node J_s to M), and diverging (from node D to O_E), as well as their interaction. As Figure 2 illustrates, for increased generality, the network under consideration is equally discretized in space except at nodes D and M where $\Delta x \neq \Delta x_D \neq \Delta x_M$. This necessitates a slight modification in the calculations presented to this point for the interrupted flow region. The changes required are

At $j = D$ (diverging area):

$$k_D^{n+1} = \frac{k_M^n \Delta x_D + k_{D-1}^n \Delta x_M}{\Delta x_D + \Delta x_M} - \frac{\Delta t(q_M^n - q_{D-1}^n)}{\Delta x_D + \Delta x_M} - g_D^n \Delta t \quad (10)$$

where the dissipation term is $g_D^n = q_{OE}^n / \Delta x_D$.

At $j = M$ (merging area):

$$k_M^{n+1} = \frac{k_{M+1}^n \Delta x_M + k_D^n \Delta x}{\Delta x_M + \Delta x} - \frac{\Delta t(q_{M+1}^n - q_D^n)}{\Delta x_M + \Delta x} + g_M^n \Delta t \quad (11)$$

where the generation term is $g_M^n = q_{JS}^n / \Delta x_M$.

At $j = D - 1$ (the node immediately upstream of D):

$$k_{D-1}^{n+1} = \frac{k_D^n \Delta x + k_{D-2}^n \Delta x_D}{\Delta x + \Delta x_D} - \frac{\Delta t(q_D^n - q_{D-2}^n)}{\Delta x + \Delta x_D} \quad (12)$$

At $j = M + 1$ (the node immediately downstream of M):

$$k_{M+1}^{n+1} = \frac{k_{M+2}^n \Delta x_M + k_M^n \Delta x}{\Delta x_M + \Delta x} - \frac{\Delta t(q_{M+2}^n - q_M^n)}{\Delta x_M + \Delta x} \quad (13)$$

At all the remaining internal nodes, the densities are obtained from Equation 1. Finally, all the corresponding speeds and flows for the above cases are obtained in the usual manner, i.e., from Equations 2 and 3.

All the needed boundary conditions, i.e., the arrival patterns at nodes O and O_s and the departure patterns at nodes J and J_E, are determined or specified as before. Further, spillback effects at node D are treated as sinks, while flow at the internal boundaries J_S and O_E is determined dynamically as described previously. Finally, it should be repeated that to keep the numerical solutions within reasonable bounds, it is necessary to maintain the relationship $\Delta x/\Delta t \rangle u_f$; this restriction also applies to Δx_D and Δx_M.

Turning Lanes

Turning lanes frequently encountered in practice present additional modelling difficulties. In this section, treatment of exclusive lanes is summarized. This involves modelling of diverging dynamics and appropriate definition of boundary conditions. Because traffic in turning lanes is diverted from the main stream, it is logical to treat the lanes as simple sinks. However, due to the length of these lanes and possible conflicts at their downstream end, they should be treated differently. As before, the state equations of the main flow and turning lanes must be solved simultaneously and their interactions (exchange of flow and momenta) considered. The conservation equation as described here takes into account the exchange of flow. Exchange of momenta must be considered only with the high order continuum models and is incorporated in the momentum equation as described in earlier publications (*4*, *14*).

When turning lanes exist, exchange of flow between the turning and through lanes is included in the generation rates $g(x, t)$ of the conservation equation. In the previous section a similar procedure was introduced for traffic sinks. However, the effective diverging area, and hence the computation of dissipation rate, was limited to only one segment Δx.

Figure 2 presents the space discretization of an intersection approach with a right turning lane R. In general, diversion of flow occurs in section $r \leq R$ of the main stream and the turning lane. Dynamic description of flow in the main lane and the turning lane begins by considering the three streams involved, i.e., the total flow q in the through lanes, its diverging component q_d, and the turning lane flow q_r. Simultaneous solution of the state equations governing these streams requires knowledge of the generation and dissipation rate $g(x, t)$, which is a function of both q and q_r. From the physics of the problem the generation rate of any segment j in section r at $t = n\Delta t$, i.e., g_j^n, should be a function of the diverging flow component $q_{j-1,d}^{n-1}$ of segment $j - 1$ at $t = (n - 1)\Delta t$. The following

relationship can be derived for dynamic determination of the generation rate at turning lanes (*11*):

$$g_j^n = \frac{q_{j-1,d}^{n-1}}{\Delta x} \frac{S_j^{n-1}}{\sum_{i=j}^{J_r} S_i^{n-1}}$$

$$= \frac{q_{j-1,d}^{n-1}}{\Delta x} \frac{(k_{\text{jam}} - k_{j,r}^{n-1})}{\sum_{i=j}^{J_r} (k_{\text{jam}} - k_{i,r}^{n-1})} \quad (14)$$

where

S_j^{n-1} = storage space available in segment j in r at $t = (n - 1)\Delta t$;
$k_{j,r}^{n-1}$ = density of node j in r at $t = (n - 1)\Delta t$; and
$q_{j-1,d}^{n-1}$ = diverging flow component.

From the above expression and Equation 5, a computational algorithm for dynamic calculation of flow on the through and turning lanes has been developed and described in detail (*11*). This takes into account both the interactions between the main and turning flows and the proper definition of boundary conditions at the stop line. For the through flow this is accomplished as in "Isolated Intersections." For the right turning flow, however, node J_R (Figure 2) should be treated in a manner similar to that of node O_E (described earlier) as the cross street flow affects right turning capacity.

As mentioned earlier, the modelling presented to this point also applies to left turning lanes. The only difference lies in defining the boundary conditions at the stop line of the turning lane, during the green interval. If traffic flow on this lane moves during an exclusive phase, then flow at the stop line is defined as in the through case described in "Isolated Intersections." Naturally, due to the lower turning speed, saturation flow and therefore capacity of the turning lane is lower than the through lanes; estimation of this capacity can easily be obtained from the *Highway Capacity Manual* (*13*). If flow on the exclusive lane moves concurrently with opposing flow, then left turning saturation flow is lower and at each time increment can be determined from the opposing flow. Estimation of left turning saturation flow with opposing traffic can also be obtained from the *Highway Capacity Manual* (*13*, Figure 10-3) or related literature (*12*, *15*). Thus, at each time step, if a queue exists, flow at the stop line of the turning lane will equal the opposed left turning saturation flow. Following queue dissipation, arrival flow at the immediately upstream node must be compared to saturation flow at that instant, and the lowest of the two will prevail.

Spillback Effects

When the flow rate on node J_R drops during green or the turning volumes are high, spillback from the turning lanes to the main stream is possible. In this case congestion propagates upstream of the stop line (node J_R), and as density in the right lane increases, the generation rate decreases. Therefore, density in the through lanes will increase as flow on the right lane becomes congested. As an extreme example, assume that due to congestion in the cross street, flow at the stop line of the turning lane is very low, resulting in compact queueing ($k \approx k_{\text{jam}}$) in this lane. As a result, the generation rate will be very low ($g \approx 0$), and the total flow at node J_B will propagate to the downstream node J_b almost unchanged, provided flow at J_b is not disrupted by downstream congestion. This implies that at congested turning flows, the spillback mechanism provided by the main turning lane algorithm is weak and should be improved. For this reason, an improved spillback algorithm was developed (*11*). Briefly, the algorithm ensures that at each time step the total through volume at J_b and the remaining through volume in Section C does not exceed the through volume passing node O_c.

Multilane and Shared Lanes Treatment

Treatment of flow on a lane-specific basis may not be needed, especially if turning lanes have already been taken into account, for if we exclude turning movements (considered earlier), little additional lane changing should be expected at the intersection. Thus, aggregate analysis of all through lanes should suffice in most practical situations. Lane-by-lane analysis can also be performed, if desired, using the general methodology presented earlier; such treatment could be justified in segments between intersections.

Analysis of multilane dynamics requires consideration of the state equations of all lanes; in the simplest case this implies one conservation equation per lane. The exchange of flow between neighboring lanes can be included in the generation term of the conservation equation. This exchange can be obtained from the observation that it is related to the density differences among lanes and other location-specific parameters. A complete modelling of multilane dynamics with its numerical implementation is presented in an earlier publication (*14*).

When no exclusive turning lanes exist, optional or shared lanes serving more than one movement are often employed. This situation is depicted on the westbound approach of the first intersection in Figure 2. Modelling during the red and yellow phases does not present any difficulty as the stop line represents a boundary on which flow is defined as in "Isolated Intersections." During green, this line is no longer a boundary and is either extended by a dummy segment (isolated case) or replaced by the upstream node of the downstream link. In either case the flow in the segment immediately after the stop line includes two dissipation terms, one for each movement. The dissipation term corresponding to the right turning movement is defined as in sinks ("Sources and Sinks"). For the left turns, the dissipation term at each instant is determined from the lowest of two values: (a) the left turning demand, which is a fraction of the total flow at the stop line, and (b) the left turning saturation flow, which is time varying when moving concurrently with opposing traffic and is determined as in left turning lanes.

When congestion builds up at the cross street, the right or left turning generation terms will reduce. To ensure spillback effects are considered, flow at the node downstream of the stop line should not be allowed to exceed the through demand, i.e., this node may become an internal boundary during green. In this case the spillback mechanism described earlier applies.

COORDINATED INTERSECTIONS

The modelling presented to this point can easily be extended to coordinated intersections. This requires modifications to

the boundary conditions at the upstream end of the coordinated links. Referring to Figure 2, it can easily be realized that the upstream boundary of a signalized link is no longer an external boundary. For instance, consider node O_A. During the EB green phase at intersection 1, O_A is treated as any ordinary node, i.e., flow on O_A is obtained from Equations 1–3 by adding one or more segments connecting O_A to the stop line upstream as shown in Figure 2b. If exclusive lanes exist on the upstream approach, flow on the nodes falling within the intersection is also computed from Equations 1–3; otherwise, if shared lanes exist, the dissipation terms of the turning movements must be considered ("Multilane and Shared Lanes Treatment"). If right turns on red are allowed from the NB approach, they can be treated as described in "Sources and Sinks" (i.e., as in sources); in such a case the generation term should be added to node $O_A - 1$.

Following the EB green phase at intersection 1, several phasing possibilities exist with varying effects on O_A. Considering the possibility of an exclusive left turning phase from the SB approach, Figure 2c applies, i.e., flow is again computed by connecting O_A to the stop line of the left turning movements and employing Equations 1–3. During the NB-SB green phase the right turning flows from the NB approach can be treated as in "Turning Lanes" (sinks); in such case node O_A is an internal boundary analogous to O_E of section E in Figure 2a. Stated otherwise, the sink treatment applies in this case where the main flow is in the NB direction. The only complexity is introduced when left turns from the SB flow are also allowed simultaneously with the right turns and through movement NB. This situation requires further modelling. Referring to Figure 2d, one sees the total flow at O_A consists of the right turning component of the NB stream and the left turning component of the SB stream. In this case flow at O_A' and the right turns have priority and are treated as before, i.e., nodes O_A' and O_A are treated as nodes D and O_E in Figure 2a, respectively. Flow at O_A'' is restricted by the total flow at O_A' and is determined as in the optional left turning case. Thus, at each time step total flow at O_A will be the sum of the turning flows at O_A' and O_A''. Because capacity at O_A is restricted by the flow at $O_A + 1$ (see "Sources and Sinks" for sinks), capacity at O_A restricts flow at O_A'' first and then at O_A'. When these restrictions are in force, nodes O_A'' and O_A' become internal boundaries to allow propagation of spillbacks.

TEST RESULTS

Testing of all the modelling details presented here requires substantial data collection at many locations over a reasonably long time. Due to the limited resources available, extensive model testing could not be performed. As an alternative to field data collection, microscopic simulation was employed to generate the data base necessary to judge the realism and estimate the expected accuracy of the proposed methodology. More specifically, the most recent version of the NETSIM (*9*) program was employed for this purpose. This program is reasonably well established and documented and has been extensively tested over the many years of its development. In addition to the comparisons against the simulated data, limited testing with field data was also performed and is presented in an earlier publication (*16*). In these earlier tests, nonlinear equilibrium u-k models were also employed including discontinuous ones, and it was concluded that although proper u-k selection can improve model performance, the linear alternative leads to acceptable accuracy levels. Prior to the comparisons with the data base, model performance was initially determined by inspection of the results, including visual checking of q, k, and u plots versus time and distance. This was very effective for screening many modelling alternatives that led to unreasonable results.

The measures of effectiveness employed to determine the overall model accuracy and the method of their computation are as follows:

Total Travel (in vehicle-miles):

$$TT = \sum_{j=1}^{J} \sum_{n=1}^{N} q_j^n \, \Delta t \, \Delta x$$

where J is the total number of nodes (excluding the dummy segment) and N is the simulation time/Δt.

Total Travel Time under Interrupted Conditions (in vehicle-minutes):

$$TTTi = \sum_{n=1}^{N} \sum_{j=1}^{J} k_j^n \, \Delta x \, \Delta t$$

Total Travel Time under Uninterrupted Flow Conditions (in vehicle-minutes):

$$TTTu = \sum_{n=1}^{N} \sum_{j=1}^{J} k_{j,u}^n \, \Delta x \, \Delta t$$

where $k_{j,u}^n$ is the density that would have been realized at node j under ideal conditions, i.e., if the signal were not present. This is obtained by assuming continuous green at the stop line of the approach being considered.

Delay (in vehicle-minutes):

$$\text{Delay} = TTTi - TTTu$$

Average Speed (in mph):

$$u = TT/TTTi$$

Total Arriving Volume (in vehicles):

$$A = \sum_{n=1}^{N} q_1^n \, \Delta t$$

Total Departing Volume (in vehicles):

$$D = \sum_{n=1}^{N} q_J^n \, \Delta t$$

The deviations of the above measures of effectiveness from the NETSIM estimates were computed and the percentage difference (PD) between them determined. In the results presented next, a positive PD indicates that the modelling proposed here overestimates the corresponding MOE compared to NETSIM; conversely, a negative PD indicates underestimation. Finally, it should be noted that the space increment necessary for obtaining reasonable accuracy was found to be in the range of 30 to 150 ft.

Space limitations do not allow presentation of all test results. For this reason, only the comparisons from two representative situations are presented. The first situation represents a straight

through link without turning movements under light, medium, and heavy flow conditions. The second one represents a coordinated link without turning movements, under varying offsets. In the second situation, for easy intuitive inspection, it is assumed no turning movements enter the link from the cross street at the upstream intersection.

Isolated Case

In this case, all through lanes are treated in an aggregate fashion; thus, the results presented and the demand pattern are per lane estimates. The link length is 2,600 ft. The arrival flow changes from 630 vehicles per hour/lane to 900, 1,170, and 360 vehicles per hour/lane every 15 min. These changes replicate a realistic peak hour demand pattern. Assuming a two-phase operation, a cycle of 60 sec, and a yellow interval of 3 sec, the green time of the approach under consideration is varied three times from 39 sec to 27 sec, generating light, medium, and heavy congestion. The average degree of saturation X corresponding to these timing plans and demand pattern is 0.66, 0.85, and 0.94, respectively. Initial conditions in each case were determined from the NETSIM (*9*) program following an initialization interval.

In earlier experimentation (*4*) the optimal step size was $\Delta x = 50$ ft and $\Delta t = 1$ sec; this step size was adopted here. Further, although nonlinear equilibrium u-k models can result in higher accuracy (*4*), the linear model was employed here to demonstrate the robustness of the proposed treatment. The model parameters, i.e., the free flow speed u_f and jam density k_{jam}, were assumed to be 34 mph and 212 vehicles per mile/lane, respectively.

Table 1 presents the results obtained from the comparisons between the model and NETSIM estimates following 1 hr of analysis. The right half of the table (columns 6–10) presents results obtained by generating the arrivals according to the stochastic process described in "Isolated Intersections" using the 15-min averages previously mentioned. The left half (columns 1–5) of the table corresponds to the NETSIM-generated arrivals that were averaged every 3 min and used for obtaining the model results. In both cases the NETSIM estimates are the same because only the boundary conditions were changed for testing the modelling proposed earlier. As expected, the

TABLE 1 COMPARISONS OF MODEL- AND NETSIM-GENERATED RESULTS

CASE / MOE		NETSIM generated arrivals					Model generated arrivals				
		X=0.66	X=0.85			X=0.94	X=0.66	X=0.85			X=0.94
			Cap=1800 Uf=34	Cap=1800 Uf=32	Cap=1636 Uf=34			Cap=1800 Uf=34	Cap=1800 Uf=32	Cap=1636 Uf=34	
MOE		(1)	(2)	(3)	(4)	(5)	(6)	(7)	(8)	(9)	(10)
TT (veh-mi.)	NETSIM	377.44	377.25	377.39	343.19	376.98	377.44	377.25	377.39	343.19	376.98
	Model	399.30	401.89	401.46	372.19	383.76	400.87	393.86	416.19	366.78	417.96
	PD (%) #	(5.8)	(6.5)	(6.4)	(8.4)	(1.8)	(6.2)	(4.4)	(10.3)	(6.9)	(10.9)
TTTi (veh-min)	NETSIM	895.61	1726.22	1715.51	1543.74	2715.47	895.61	1726.22	1715.51	1543.74	2715.47
	Model	1026.23	1822.75	1784.84	1620.41	2883.83	1034.98	1787.05	1920.89	1695.85	3126.95
	PD (%)	(14.6)	(5.6)	(4.0)	(5.0)	(6.2)	(15.6)	(3.5)	(12.0)	(9.8)	(15.2)
TTTu (veh-min)	Model	806.84	806.78	848.00	746.64	760.91	811.33	791.31	882.15	740.11	939.94
Delay (veh-min)	NETSIM	223.70	1063.03	1009.47	954.84	2073.89	223.70	1063.03	1009.47	954.84	2073.89
	Model	219.39	1015.97	936.85	873.77	2122.92	223.66	995.73	1038.74	955.73	2187.01
	PD (%)	(-1.9)	(-4.4)	(-7.2)	(-8.5)	(2.4)	(0.0)	(-6.3)	(2.9)	(0.1)	(5.4)
Average Speed (mph)	NETSIM	25.30	13.14	13.23	13.39	8.38	25.30	13.14	13.23	13.39	8.38
	Model	23.35	13.23	13.50	13.78	7.98	23.24	13.22	13.00	12.98	8.02
	PD (%)	(-7.7)	(0.7)	(2.0)	(2.9)	(-4.8)	(-8.1)	(0.6)	(-1.7)	(-3.1)	(-4.3)
Total Arrivals (veh)	NETSIM	763.50	763.10	763.20	694.30	763.00	763.50	763.10	763.10	694.30	763.20
	Model	763.70	763.80	753.80	703.60	746.70	767.00	746.20	782.20	699.50	894.60
	PD (%)	(0.0)	(0.0)	(-1.2)	(1.3)	(-2.1)	(0.4)	(-2.2)	(2.5)	(0.7)	(17.2)
Total Departures (veh)	NETSIM	769.50	769.40	770.20	700.30	763.40	769.50	769.40	770.20	700.30	763.40
	Model	843.00	780.50	782.60	718.90	735.10	844.30	773.40	803.40	710.10	754.90
	PD (%)	(9.6)	(1.4)	(1.6)	(2.7)	(-3.7)	(9.7)	(0.5)	(4.3)	(1.4)	(-1.1)

* Results above correspond to one hour simulation.

\# PD (%) = percentage of difference from data = (Model-NETSIM)/NETSIM * 100%

results of the left half of the table are closer to the NETSIM data, although both are equally satisfactory.

Columns 2–4 and 7–9 corresponding to $X = 0.85$ include two additional values of u_f and capacity affecting the equilibrium u-k relationship to demonstrate the model sensitivity to this relationship. As the table suggests, although model performance deteriorates, the results are still acceptable. To be sure, all the estimates obtained by the model are satisfactory as they deviate mostly well below 10 percent from the NETSIM data. When the degree of saturation increases, model performance improves; this suggests that the proposed modelling is more appropriate for congested flows.

Before concluding, it should be noted that with respect to uninterrupted total travel time $TTTu$, the differences between the model results and NETSIM were more pronounced. This is because of the difference in the method of calculating $TTTu$. According to NETSIM, $TTTu$ or "ideal travel time" is estimated according to a "target speed" for the link; however, no further information on this speed is included in the program documentation, and nothing is mentioned about the existence of the signal and how it is taken into account in the calculations.

Signalized Links

During the testing of oversaturated coordinated links, it was quickly realized that for the reasons mentioned later in this section, NETSIM in its present form is not suitable for generating a reliable data base, i.e., it does not treat oversaturated signalized links effectively. Therefore, the effectiveness of the model can only be judged by intuitive inspection of the results. Two test cases are presented here: one demonstrating a spillback to the upstream link and another without spillback. As in the isolated case, all through lanes are treated in an aggregate fashion. As such, the results presented here pertain to per lane estimates. A two-phase operation of a one-way signalized link is assumed with a base cycle length of 150 sec and a yellow interval of 3 sec. The layout is as in the EB direction of Figure 2a; however, no side streets and turning lanes are taken into account in these test cases. The arrival flow begins at 864 vph/lane (capacity is 1,800 vph/lane) for 15 min and drops to 576 vph/lane for another 15 min. The green times are 90 sec and 60 sec at the first and second intersections, respectively. The average degree of saturation corresponding to this time plan and demand pattern is 0.80 for the upstream link and 1.20 for the downstream link. A two-cycle initialization period, with a flow of 720 vehicles per hour/lane, was used to define initial conditions. A free flow speed of 40 mph and a jam density of 180 vehicles per mile/lane were assumed. The step size for both cases is $\Delta x = 60$ ft and $\Delta t = 1$ sec. As noted previously, no turning movements are assumed in this example; this implies no input to the upstream end of the signalized link during red, for easy intuitive inspection of the formation and dissipation of congestion.

In the first case, the signalized link length is assumed to be 2,000 ft; this represents the case in which no spillback occurs. Spillback results when the queue from the downstream link extends into the upstream link. In the second case, the signalized link length is 1,500 ft; this represents spillback of congestion during the test period. In both cases, the offsets are increased in steps from zero with a step size approximately one quarter of a cycle. The test runs are for a period of half an hour. The results indicated that in the second case, the queue from the downstream signal backs up into the upstream link in the fourth cycle. The spillback recedes after five cycles (i.e., in the ninth cycle) due to the lower arrivals into the system after the first 15-min. interval.

The test runs also indicated that the offsets do not significantly affect the model results (MOEs) such as total travel, total travel time, and average speed, while total arrivals and departures are the same. When an attempt was made to verify this result by NETSIM, it was realized that this program presently cannot effectively treat oversaturated signalized links. This is because the NETSIM results demonstrated great variability with change in offsets. This latter result does not agree with experience and intuition according to which at high saturation levels, such as those presented, offsets should not produce such large differences, i.e., they should not significantly affect the MOEs. Part of the problem lies with the NETSIM program, which presently does not deal with severe congestion. For instance, when the upstream end of the link is reached, NETSIM begins to store cars vertically ignoring space and spillback effects. Improvements to the NETSIM program are being made to take spillback effects and severe congestion into account.

A visual depiction of the model's performance is seen in Figure 3, which shows the density plots versus space and time for both cases. The plot includes the cycles at which congestion is maximum. In the first case congestion barely reaches the upstream intersection, while in the second case it spreads to the upstream link. The blank spaces in Figure 3 are generated because, as explained earlier, no input occurs during the red phase to the signalized link to allow some dissipation of congestion. In this manner the trajectory of the queues becomes clearer and their evolution easier to track. Finally, compression and dispersion characteristics are manifested.

CONCLUDING REMARKS

In this paper an attempt was made to treat traffic flow at congested intersections and arterials in a unified and consistent macroscopic fashion. This was done without ignoring important components and characteristics of urban streets and making the oversimplifications usually encountered in practical and theoretical models. Major advantages of the approach taken here are the explicit inclusion of both time and space and compressibility characteristics. Unlike empirical models, these characteristics are not induced artificially, but are inherent in the modelling.

Another consideration concerning the usefulness of the modelling presented here is that it can be implemented in microcomputers. This is because of the simplicity of the numerical schemes employed and the macroscopic nature of the models, which allow efficient computations and minimal memory requirements. The test results were in fact obtained by implementing the proposed methodology in IBM-PC-based software. Similar modelling was employed in an earlier interactive microcomputer-based simulation program for freeways (*17*).

The testing presented here and testing against actual field data presented in an earlier publication (*16*) are limited. Although this earlier testing included more complex equilibrium models (nonlinear and discontinuous ones), more testing is needed for model refinement and verification. This could

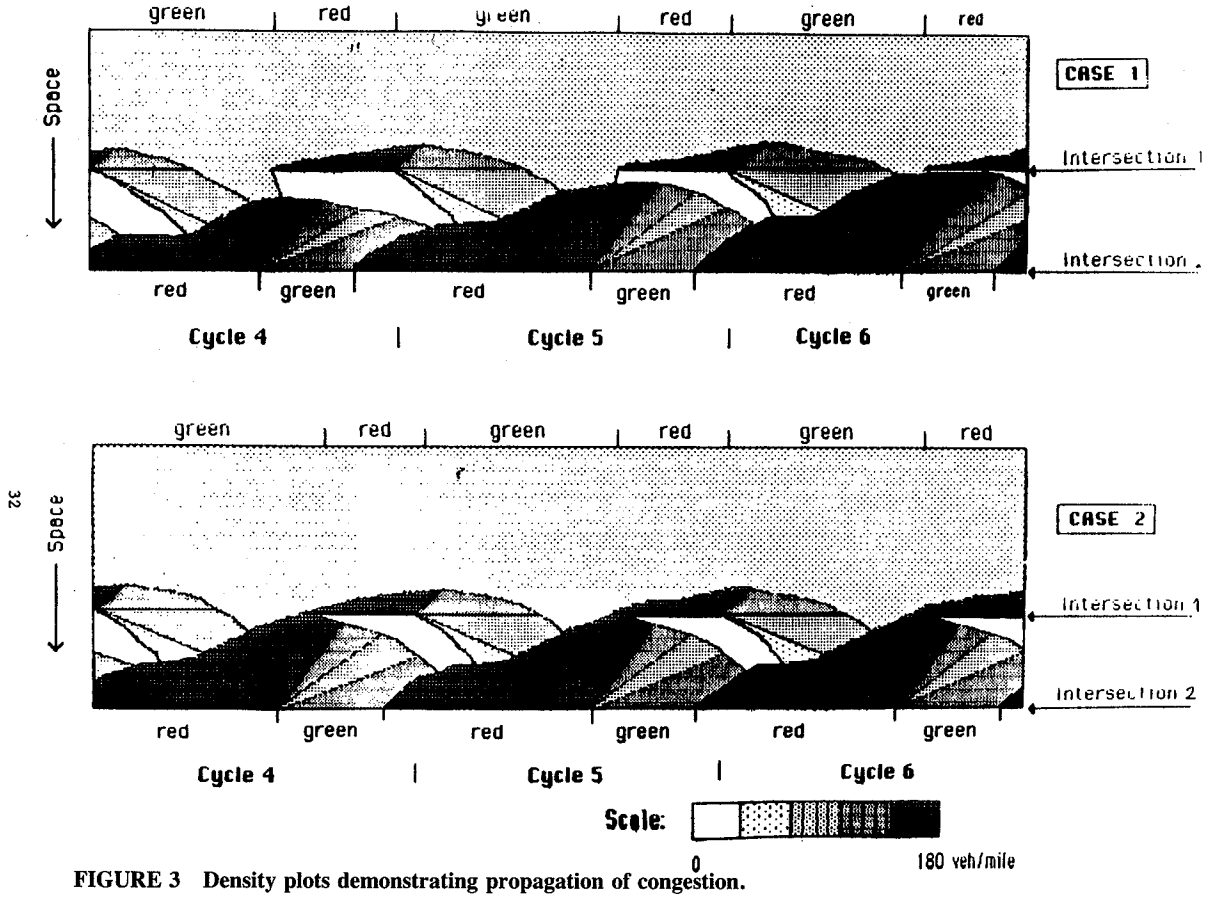

FIGURE 3 Density plots demonstrating propagation of congestion.

lead to simplifications that are probably necessary for more widespread practical implementation of the methodology presented here. Although the computational requirements of the proposed modelling are substantially lower than those of microscopic models, they are probably higher than empirical models. A sacrifice in computational effort, however, should be expected for more detail, accuracy, and realism.

ACKNOWLEDGMENTS

Financial support for this research was provided by the National Science Foundation and by the Exxon Petroleum Violations Escrow Fund as administered through the U.S. Department of Energy.

REFERENCES

1. M. H. Lighthill and G. B. Whitham. On Kinematic Waves-II. A Theory of Traffic Flow on Long Crowded Roads. *Proceedings, Royal Society* (London), A229, No. 1178, 1955, pp. 317–345.
2. H. J. Payne. Models of Freeway Traffic and Control. *Proc., Mathematics of Public Systems, Simulation Council*, Vol. 1, No. 1, 1971, pp. 51–61.
3. W. F. Phillips. A New Continuum Traffic Model Obtained from Kinetic Theory. *IEEE Transactions on Automic Control*, Vol. AC-23, No. 2, 1978, pp. 1032–1036.
4. J. Lin. *Modelling and Analysis of Traffic Flow in Complex Transportation Networks*. Ph.D. dissertation. Department of Civil and Mineral Engineering, University of Minnesota, Minneapolis, 1985.
5. G. Stephanopoulos and P. G. Michalopoulos. Modelling and Analysis of Traffic Queue Dynamics at Signalized Intersections. *Transportation Research*, Vol. 13A, 1979, pp. 295–307.
6. P. G. Michalopoulos, G. Stephanopoulos, and V. B. Pisharody. Modelling of Traffic Flow at Signalized Links. *Transportation Science*, Vol. 14, No. 1, 1980, pp. 9–41.
7. P. G. Michalopoulos and V. B. Pisharody. Platoon Dynamics on Signal Controlled Arterials. *Transportation Science*, Vol. 14, No. 4, 1980, pp. 365–396.
8. B. D. Greenshields. A Study of Traffic Capacity. *HRB Proc.*, Vol. 14, 1934, pp. 448–477.
9. *Traffic Network Analysis with NETSIM—A User Guide*. Implementation Package FHWA-IP-80-3. FHWA, U.S. Department of Transportation, 1980.
10. D. L. Gerlough and M. J. Huber. *Special Report 165—Traffic Flow Theory: A Monograph*. TRB, National Research Council, Washington, D.C., 1975.
11. P. G. Michalopoulos and L. Wung. *Treatment of Interrupted Traffic Flow in Complex Congested Arterials*. Department of Civil and Mineral Engineering, University of Minnesota, Minneapolis, 1986.
12. J. C. Tanner. A Theoretical Analysis of Delays at an Uncontrolled Intersection. *Biometrika 49*, 1962, pp. 163–170.
13. *Special Report 209: Highway Capacity Manual*. TRB, National Research Council, Washington, D.C., 1985.
14. P. G. Michalopoulos, D. E. Beskos, and Y. Yamauchi. Multilane Traffic Flow Dynamics: Some Macroscopic Considerations. *Transportation Research*, 18B, No. 4/5, 1984, pp. 377–395.
15. P. G. Michalopoulos, J. O'Connor, and S. M. Novoa. Estimation of Left-Turn Saturation Flows. In *Transportation Research Record 667*, TRB, National Research Council, Washington, D.C., 1977, pp. 35–41.
16. P. G. Michalopoulos, D. E. Beskos, and J. Lin. Analysis of Interrupted Traffic Flow by Finite Difference Methods. *Transportation Research*, 18B, No. 4/5, 1984, pp. 409–421.
17. P. G. Michalopoulos and J. Lin. A Freeway Simulation Program for Microcomputers. *Proc., 1st National Conference on Microcomputers in Urban Transportation*, San Diego, Calif., 1985, pp. 330–341.

Publication of this paper sponsored by Committee on Traffic Flow Theory and Characteristics.